

# Generic Contrast Agents

Our portfolio is growing to serve you better. Now you have a *choice*.



[VIEW CATALOG](#)

# AJNR

This information is current as of May 4, 2025.

## **Thin-Slice Pituitary MRI with Deep Learning–Based Reconstruction for Preoperative Prediction of Cavernous Sinus Invasion by Pituitary Adenoma: A Prospective Study**

M. Kim, H.S. Kim, J.E. Park, S.Y. Park, Y.-H. Kim, S.J. Kim, J. Lee and M.R. Lebel

*AJNR Am J Neuroradiol* 2022, 43 (2) 280-285

doi: <https://doi.org/10.3174/ajnr.A7387>

<http://www.ajnr.org/content/43/2/280>

# Thin-Slice Pituitary MRI with Deep Learning–Based Reconstruction for Preoperative Prediction of Cavernous Sinus Invasion by Pituitary Adenoma: A Prospective Study

 M. Kim,  H.S. Kim,  J.E. Park,  S.Y. Park,  Y.-H. Kim,  S.J. Kim,  J. Lee, and  M.R. Lebel



## ABSTRACT

**BACKGROUND AND PURPOSE:** Accurate radiologic prediction of cavernous sinus invasion by pituitary adenoma remains challenging. We aimed to assess whether 1-mm-slice-thickness MRI with deep learning–based reconstruction can better predict cavernous sinus invasion by pituitary adenoma preoperatively and to estimate the depth of invasion and degree of contact in relation to the carotid artery, compared with 3-mm-slice-thickness MRI.

**MATERIALS AND METHODS:** This single-institution, prospective study included 67 consecutive patients (mean age, 53 [SD, 12] years; 28 women), between January and August 2020, who underwent a combined contrast-enhanced T1-weighted imaging protocol of 1-mm-slice-thickness MRI + deep learning–based reconstruction and 3-mm-slice-thickness MRI. An expert neuroradiologist who was blinded to the imaging protocol determined cavernous sinus invasion using the modified Knosp classification on 1-mm-slice-thickness MRI + deep learning–based reconstruction and 3-mm-slice-thickness MRI, respectively. Reference standards were established by the consensus of radiologic, intraoperative, pathologic, and laboratory findings. The primary end point was the diagnostic performance of each imaging protocol, and the secondary end points included depth of invasion and degree of contact in relation to the carotid artery.

**RESULTS:** The diagnostic performance of 1-mm-slice-thickness MRI + deep learning–based reconstruction (area under the curve, 0.79; 95% CI, 0.69–0.89) in predicting cavernous sinus invasion by pituitary adenoma was higher than that of 3-mm-slice-thickness MRI (area under the curve, 0.61; 95% CI, 0.52–0.70;  $P < .001$ ). One-millimeter-slice-thickness MRI + deep learning–based reconstruction demonstrated greater depth of invasion by pituitary adenomas from the medial intercarotid line than 3-mm-slice-thickness MRI (4.07 versus 3.12 mm,  $P < .001$ ). A higher proportion of cases were in a greater degree of contact with the intracavernous ICA with 1-mm-slice-thickness MRI + deep learning–based reconstruction than with 3-mm-slice-thickness MRI (total encasement, 37.3% versus 13.4%,  $P < .001$ ;  $>270^\circ$ , 38.8% versus 16.4%,  $P < .001$ ).

**CONCLUSIONS:** Compared with 3-mm-slice-thickness MRI, 1-mm-slice-thickness MRI + deep learning–based reconstruction showed a higher diagnostic performance in preoperatively predicting cavernous sinus invasion by pituitary adenomas and demonstrated a greater depth and degree of contact in relation to the carotid artery.

**ABBREVIATIONS:** AUC = area under the receiver operating characteristic curve; CNN = convolutional neural network; DLR = deep learning–based reconstruction; 1-mmMRI = 1-mm-slice-thickness MRI without deep learning–based reconstruction; 3-mmMRI = 3-mm-slice-thickness MRI; 1-mmMRI+DLR = 1-mm-slice-thickness MRI with deep learning–based reconstruction; TSA = transsphenoidal approach


**P**reoperative evaluation of cavernous sinus invasion by a pituitary adenoma is important for establishing the safest and most effective treatment strategy for patients. Surgical resection by a transsphenoidal approach (TSA) is the first-line treatment for most macroadenomas,<sup>1,2</sup> and accurate evaluation of cavernous sinus invasion is crucial to avoid injury to the ICA and

cranial nerves.<sup>3–5</sup> Complete resection of pituitary adenomas is recommended to achieve endocrinologic remission for a functioning pituitary adenoma and to lower the rate of recurrence, while incomplete resection followed by radiation therapy may be recommended for pituitary adenomas with cavernous sinus invasion.<sup>4,6,7</sup>

Received March 17, 2021; accepted after revision October 9.

From the Department of Radiology and Research Institute of Radiology (M.K., H.S.K., J.E.P., S.J.K.), Departments of Clinical Epidemiology and Biostatistics (S.Y.P.), and Neurosurgery (Y.-H.K.), University of Ulsan College of Medicine, Asan Medical Center, Seoul, Korea; GE Healthcare (J.L.), Seoul, Korea; GE Healthcare (M.R.L.), Calgary, Alberta, Canada; and Department of Radiology (M.R.L.), University of Calgary, Calgary, Alberta, Canada.

Please address correspondence to Ho Sung Kim, MD, PhD, Department of Radiology and Research Institute of Radiology, University of Ulsan College of Medicine, Asan Medical Center 88 Olympic-ro 43-gil, Songpa-Gu, Seoul 05505, South Korea; e-mail: radhskim@gmail.com

 Indicates article with online supplemental data.  
<http://dx.doi.org/10.3174/ajnr.A7387>

Radiologic evaluation of cavernous sinus invasion relies on delineating the morphologic relationship between the pituitary adenoma and the cavernous sinus.<sup>8</sup> In particular, parasellar extension of the pituitary adenoma in relation to the lines drawn between the intracavernous and supracavernous ICAs underlies the modified Knosp classification, which is the most commonly used criteria for evaluating cavernous sinus invasion radiologically.<sup>8,9</sup> While MR imaging with 2- to 3-mm slice thickness is commonly used for pituitary imaging,<sup>10</sup> evaluation of parasellar extension by a pituitary adenoma remains challenging due to the inherently small size of the sellar fossa and delicate anatomy of the cavernous sinus.

A previous study by our group showed that high-spatial-resolution pituitary imaging may be achieved by applying deep learning-based reconstruction (DLR) to thin-slice MR imaging and demonstrated its diagnostic value in a postoperative setting.<sup>11</sup> Reducing the slice thickness is inevitably accompanied by an increased noise level, decreasing the signal-to-noise ratio and degrading the image quality. A novel deep learning-based MR image reconstruction pipeline based on a deep convolutional neural network (CNN) was used to provide denoising, reduce truncation artifacts, and improve edge sharpness.<sup>12</sup> It was trained with a supervised learning approach using pairs of images representing near-perfect and conventional MR images, and its technical performance has been previously reported.<sup>11,12</sup> DLR can be easily applied to the 2D spin-echo sequence commonly used in pituitary imaging, and we hypothesized that DLR may be applied to 1-mm-slice-thickness MR imaging (1-mmMRI) to enable better delineation of the morphologic relationship between a pituitary adenoma and the cavernous sinus.

The aim of this study was to assess whether 1-mm-slice-thickness MR imaging with deep learning-based reconstruction (1-mmMRI+DLR) can better predict cavernous sinus invasion by a pituitary adenoma preoperatively and estimate the depth of invasion and degree of contact in relation to the carotid artery, compared with 3-mm-slice-thickness MR imaging (3-mmMRI).

## MATERIALS AND METHODS

### Participants

This prospective study (clinicaltrials.gov, NCT04268251) was approved by the institutional review board of Asan Medical Center before patient enrollment, and written informed consent was obtained from all patients. Seventy-six consecutive patients undergoing brain MR imaging for preoperative evaluation of pituitary adenomas between January 2020 and August 2020 were enrolled in this study and underwent a combined imaging protocol of 1-mmMRI+DLR and 3-mmMRI within 24 hours before TSA. The primary end point was the diagnostic performance of 1-mmMRI+DLR and 3-mmMRI in preoperatively predicting cavernous sinus invasion. Secondary end points included the depth of invasion and degree of contact by a pituitary adenoma in relation to the carotid artery.

Patients whose pathologic diagnosis was not pituitary adenoma ( $n=4$ ), patients who failed to undergo the combined MR imaging protocol ( $n=3$ ), and patients whose operation was cancelled ( $n=2$ ) were excluded from the study, leaving 67 patients for final inclusion.

### MR Imaging Acquisition Protocol

MR imaging was performed with a 3T system (Signa Architect; GE Healthcare) using a 48-channel head coil. All patients underwent the MR imaging protocol dedicated to the pituitary gland within 1 month before TSA, which included the following: sagittal T1-weighted imaging: TR/TE, 611/13 ms; flip angle, 90°; FOV, 200 × 200 mm; matrix, 260 × 260; slice thickness, 3 mm with no gap; scan time, 3 minutes 40 seconds; coronal T2-weighted imaging: TR/TE, 4197/90 ms; flip angle, 90°; FOV, 180 × 180 mm; matrix, 360 × 360; slice thickness, 3 mm with no gap; scan time, 2 minutes 52 seconds; coronal T1-weighted imaging: TR/TE, 500/13 ms; flip angle, 90°; FOV, 180 × 180 mm; matrix, 260 × 260; slice thickness, 3 mm with no gap; scan time, 3 minutes; sagittal contrast-enhanced T1-weighted imaging: TR/TE, 611/13 ms; flip angle, 90°; FOV, 200 × 200 mm; matrix, 260 × 260; slice thickness, 3 mm with no gap; scan time, 3 minutes 40 seconds; axial contrast-enhanced T1-weighted imaging: TR/TE, 467/17 ms; flip angle, 90°; FOV, 230 × 185 mm; matrix, 300 × 224; slice thickness, 4 mm with 2-mm gap; scan time, 2 minutes 33 seconds; and coronal contrast-enhanced T1-weighted imaging: TR/TE, 500/13 ms; flip angle, 90°; FOV, 180 × 180 mm; matrix, 260 × 260; slice thickness, 3 mm with no gap; scan time, 3 minutes.

All patients underwent an additional MR imaging protocol for preoperative evaluation of pituitary adenoma within 24 hours before TSA, which included the following: sagittal contrast-enhanced T1-weighted imaging: TR/TE, 611/13 ms; flip angle, 90°; FOV, 200 × 200 mm; matrix, 260 × 260; slice thickness, 3 mm with no gap; scan time, 3 minutes 40 seconds; coronal contrast-enhanced T1-weighted imaging: TR/TE, 500/13 ms; flip angle, 90°; FOV, 180 × 180 mm; matrix, 260 × 260; slice thickness, 3 mm with no gap; scan time, 3 minutes; and coronal contrast-enhanced T1-weighted imaging: TR/TE, 698/16 ms; flip angle, 90°; FOV, 180 × 180 mm; matrix, 320 × 260; slice thickness, 1 mm with no gap; scan time, 4 minutes 8 seconds.

### DLR

A vendor-supplied prototype version of DLR (AIR Recon DL; GE Healthcare) was used to reconstruct the 1-mm-slice-thickness images. Development of the image reconstruction pipeline and performance of the phantom and in vivo studies have been previously reported.<sup>11,12</sup> In brief, the pipeline took raw  $k$ -space data of 1-mm-slice thickness imaging as its input and generated high-fidelity images as its output.<sup>12</sup> It was designed to offer a user-tunable reduction in image noise, truncation artifacts, and edge blurring. By means of a supervised learning approach, the CNN was trained with pairs of images representing near-perfect and conventional MR images. The near-perfect training data were high-resolution images with minimal ringing artifacts and extremely low noise levels, while the conventional training data were synthesized from near-perfect images to create lower-resolution versions with increased ringing artifacts and higher noise levels. A training data base of 4 million unique image/augmentation combinations was available to ensure the generalizability and robustness of the CNN across all anatomies; image augmentation including rotations and flips, intensity gradients, phase manipulations, and additional Gaussian noise were applied. The network was trained with gradient back-propagation via the Adam optimizer.

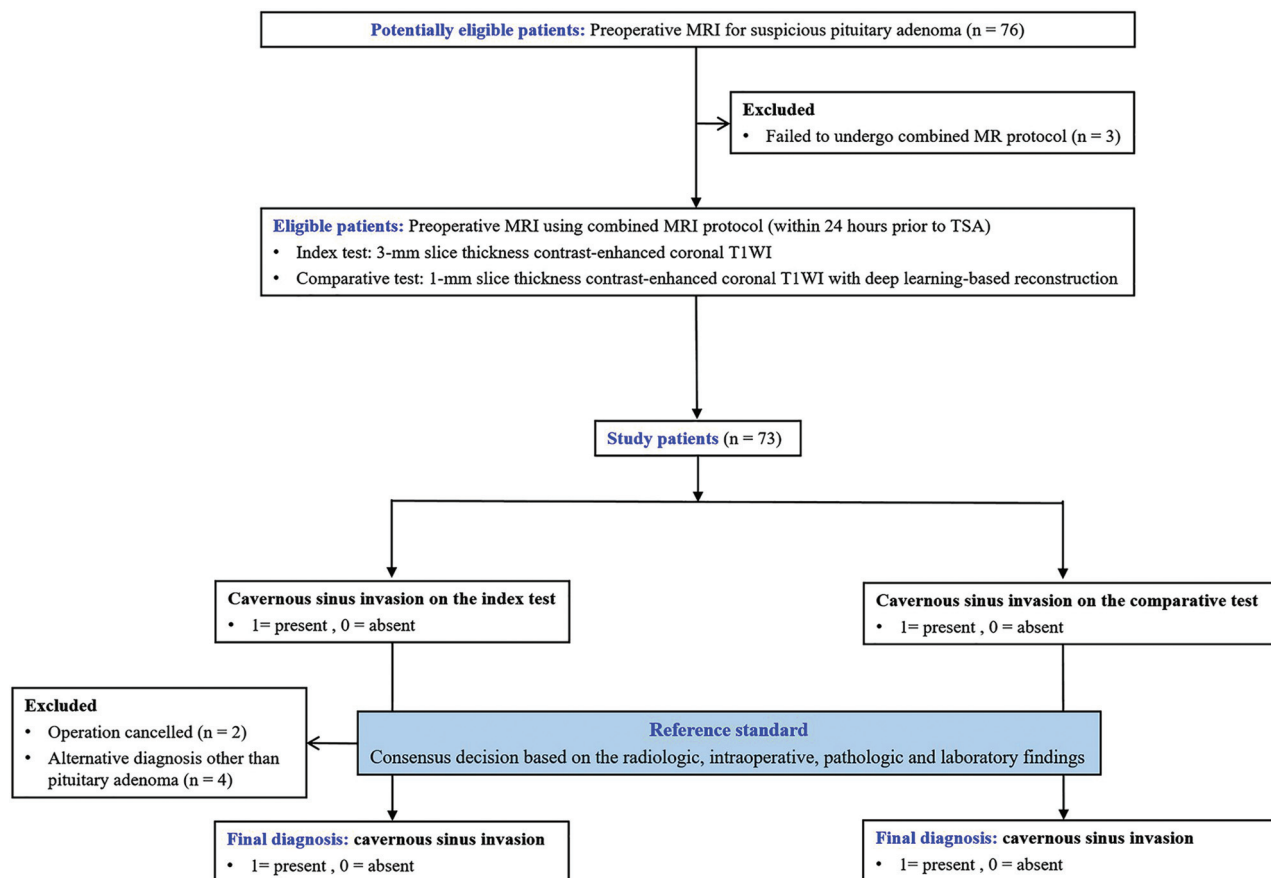


**FIG 1.** Patient inclusion process and image analysis.

### Image Analysis

Image analysis for preoperatively predicting cavernous sinus invasion was performed when preoperative MR imaging with a combined imaging protocol of 1-mmMRI+DLR and 3-mmMRI was performed within 24 hours before TSA. Image analysis was performed by an expert neuroradiologist (M.K., with 6 years of experience in neuroradiology), who was blinded to clinical information and the imaging protocol (1-mm MRI+DLR versus 3-mmMRI) in accordance with the method described in the previous study, which demonstrated good interobserver agreement in diagnosing cavernous sinus invasion.<sup>11</sup> MR imaging set 1 consisted of 3-mm-slice-thickness contrast-enhanced sagittal T1WI and 3-mm-slice-thickness contrast-enhanced coronal T1WI, and MR imaging set 2 consisted of 3-mm-slice-thickness contrast-enhanced sagittal T1WI and 1-mm-slice-thickness contrast-enhanced coronal T1WI with DLR for each patient. The reader was asked to determine cavernous sinus invasion (0 = absent, 1 = present) on MR imaging sets 1 and 2 presented in a random order according to the modified Knosp classification (0, 1, 2, 3A, 3B, and 4).<sup>9</sup> The modified Knosp classification relies on the extent of parasellar extension in relation to the lines connecting the medial, central, and lateral aspects of the cross-section of the intracavernous and supracavernous ICAs, with further subclassification depending on the involvement of the superior and inferior ICA compartments into grades 3A and 3B.<sup>9</sup> While different outcomes in terms of invasiveness, rate of gross total resection, and endocrinologic remission have been

demonstrated between grades 3A and 3B, no consensus currently exists as to the optimal cutoff for determining cavernous sinus invasion, and grades 3A and 3B were both applied.<sup>9</sup>

The reader was also asked to estimate the depth of invasion by measuring the maximal parasellar extension of the pituitary adenoma in millimeters in relation to the medial intercarotid line and to assess the degree of contact of the pituitary adenoma with the intracavernous ICA (0 = no contact, 1 = <90°, 2 = <180°, 3 = <270°, 4 = <360°, 5 = total encasement). When bilateral cavernous sinus invasion was suspected, the cavernous sinus with a higher suspicion of invasion was evaluated. Before patient enrollment, the reader underwent a training session with an experienced neuroradiologist (H.S.K., with 22 years of experience in neuroradiology) for the modified Knosp classification and determination of cavernous sinus invasion. During training, typical and difficult examples of cavernous sinus invasion and each modified Knosp classification were shown, and methods for assessing the depth of invasion in relation to the medial intercarotid line and degree of contact with the intracavernous ICA were demonstrated. Figure 1 summarizes the patient inclusion process and image analysis.

### Reference Standards

Reference standards for cavernous sinus invasion were established by the consensus of the neuroradiologist, neurosurgeons, pathologists, and endocrinologists based on radiologic, intraoperative, pathologic, and laboratory findings. An experienced neuroradiologist

**Table 1: Clinical characteristics of the patients<sup>a</sup>**

Characteristics	
Total	67
Age (yr)	53 (SD, 12)
No. of female patients	28 (42)
Functioning adenoma	14 (21)
Prolactin	5 (7.5)
Growth hormone	7 (10)
Adrenocorticotrophic hormone	1 (1.5)
Thyroid stimulating hormone	1 (1.5)
CS invasion by reference standard	29 (43)
Residual tumor following operation determined by follow-up MR imaging	11 (16)
Postoperative stereotactic radiation therapy	7 (10)

**Note:**—CS indicates cavernous sinus.

<sup>a</sup> Data are expressed as the mean (SD) or numbers with percentages in parenthesis.

(H.S.K.), who was blinded to the image analysis by the reader of the study, independently evaluated preoperative MR images as well as immediate postoperative and subsequent follow-up MR images for radiologic evaluation of cavernous sinus invasion. Two neurosurgeons explicitly documented or verbally communicated the intraoperative evaluation of cavernous sinus invasion in each patient as present, absent, or indeterminate. The cases in which the radiologic and intraoperative findings were discrepant were discussed at interdepartmental meetings. The pathologic report was reviewed for documentation of sinus or dural invasion, and endocrinologic remission was evaluated for the cases of functioning pituitary adenoma. The patients with residual pituitary adenoma on follow-up MR images or without endocrinologic remission requiring subsequent treatment were noted. The final decision on the presence or absence of cavernous sinus invasion was made by incorporating radiologic, intraoperative, pathologic, and laboratory findings in a multidisciplinary approach.

### Statistical Analysis

Previous studies reported the diagnostic performance of radiologically predicting cavernous sinus invasion with the area under the receiver operating characteristic curve (AUC) of up to 0.83.<sup>8,9,13</sup> Sample size calculation showed that 76 individuals are needed with a significance level of 5% ( $\alpha = .05$ ) and a power of 80% ( $\beta = 0.2$ ) to improve the diagnostic performance of predicting cavernous sinus invasion from an AUC of 0.83 to 0.93. To evaluate the diagnostic performance of the 1-mmMRI+DLR and 3-mmMRI in diagnosing cavernous sinus invasion, we calculated the AUC, sensitivity, specificity, positive predictive value, and negative predictive value. The comparison of the AUCs was performed by the DeLong test. Because a previous study demonstrated a difference in invasiveness between pituitary adenomas with extension into the superior and inferior compartments of the cavernous sinus,<sup>9</sup> diagnostic performances with the modified Knosp classification  $\geq 3B$  and  $\geq 3A$  as cavernous sinus invasion were calculated separately. The depth of invasion assessed on the 1-mmMRI+DLR and 3-mmMRI was compared using a paired *t* test. Evaluation of the degree of contact of pituitary adenomas with the intracavernous ICA was compared using the McNemar test.  $P < .05$  was considered indicative of a statistically significant difference. Statistical analyses were performed using R statistical and computing software (Version 3.6.1; <http://www.r-project.org>).

## RESULTS

### Patient Characteristics

Clinical characteristics of the patients are shown in Table 1. A total of 67 patients (mean age, 53 [SD, 12] years; 28 women, 42%) were enrolled, and all patients underwent resection of the pituitary adenoma by a transsphenoidal approach within 24 hours. There were 14 patients (21%) with functioning pituitary adenomas, which included 5 prolactinomas (7.5%), 7 growth hormone–releasing pituitary adenomas (10%), 1 adrenocorticotrophic hormone–releasing pituitary adenoma (1.5%), and 1 thyroid stimulating hormone–releasing pituitary adenoma (1.5%). There were 29 pituitary adenomas (43%) with cavernous sinus invasion by the reference standard. All patients underwent  $\geq 1$  immediate postoperative or follow-up MR imaging, and 11 patients (16%) were shown to have residual tumor. Seven patients (10%) underwent postoperative stereotactic radiation therapy for presumed residual tumor.

### Diagnosis of Cavernous Sinus Invasion on 3-mmMRI and 1-mmMRI+DLR

The diagnostic performance of 3-mmMRI, 1-mmMRI, and 1-mmMRI+DLR in preoperatively diagnosing cavernous sinus invasion is presented in the Online Supplemental Data. The diagnostic performance of 1-mmMRI+DLR (AUC = 0.79; 95% CI, 0.69–0.89) was higher than that of 3-mmMRI (AUC = 0.61; 95% CI, 0.52–0.70;  $P < .001$ ) and 1-mmMRI (AUC = 0.62; 95% CI, 0.49–0.74;  $P < .001$ ) according to the modified Knosp classification when grades 3B and 4 were considered as cavernous sinus invasion. When grade 3A, 3B, and 4 were considered as cavernous sinus invasion, the diagnostic performance of 1-mmMRI+DLR (AUC = 0.80; 95% CI, 0.70–0.90) showed a trend toward higher diagnostic performance than 3-mmMRI (AUC = 0.74; 95% CI, 0.64–0.85;  $P = .24$ ) and 1-mmMRI (AUC = 0.77; 95% CI, 0.65–0.86;  $P = .15$ ), without statistical significance. The modified Knosp classifications of 3-mmMRI, 1-mmMRI, and 1-mmMRI+DLR are shown in the Online Supplemental Data. The images of cavernous sinus invasion demonstrated on 1-mmMRI+DLR but not on 3-mmMRI are shown in Fig 2.

### Evaluation of the Depth of Invasion and Degree of Contact with the Intracavernous ICA by Pituitary Adenoma on 3-mmMRI and 1-mmMRI+DLR

The depth of invasion and degree of contact by pituitary adenomas with the intracavernous ICA evaluated on 3-mmMRI and 1-mmMRI+DLR are presented in Table 2. The depth of invasion of pituitary adenomas measured from the medial intercarotid line was higher on 1-mmMRI+DLR (4.07 mm; 95% CI, 3.35–4.80 mm) than on 3-mmMRI (3.12 mm; 95% CI, 2.44–3.81 mm;  $P < .001$ ) and 1-mmMRI (3.82 mm; 95% CI, 3.10–4.55 mm;  $P = .004$ ). The proportion of cases identified as the intracavernous ICA totally encased by the pituitary adenoma was higher on 1-mmMRI+DLR (25/67, 37.3%) than on 3-mmMRI (9/67, 13.4%;  $P < .001$ ) and 1-mmMRI (13/67, 19.4%;  $P = .02$ ). The proportion of cases identified as the intracavernous ICA of  $>270^\circ$  in contact with the pituitary adenoma was higher on 1-mmMRI+DLR (26/67, 38.8%) than on 3-mmMRI (11/67, 16.4%;  $P < .001$ ) and 1-mmMRI (15/67, 22.4%;  $P = .04$ ), and the proportion of cases identified as the intracavernous ICA of  $>180^\circ$  in contact with pituitary adenomas was higher on 1-



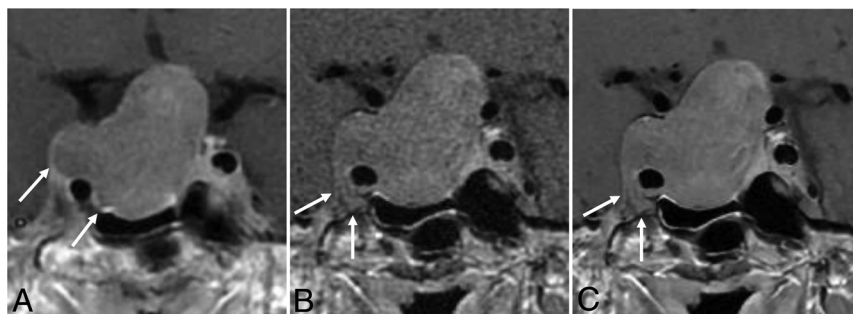


**FIG 2.** A 55-year-old man who underwent a combined MR imaging protocol for preoperative evaluation of pituitary adenoma. On a 3-mmMRI, coronal, contrast-enhanced T1-weighted image (A), the tumor is present beyond the lateral intercrotid line (modified Knosp classification 3A) and is about 180° in contact with the intracavernous ICA. One-mmMRI, coronal, contrast-enhanced T1-weighted image (B) was reconstructed using DLR (C), and the tumor is shown to encase the intracavernous ICA (arrows, modified Knosp classification 4).

**Table 2: Depth of invasion and degree of contact with the intracavernous ICA by pituitary adenoma on 3-mmMRI, 1-mmMRI and 1-mmMRI with DLR<sup>a</sup>**

	3-mmMRI	P Value	1-mmMRI	P Value	1-mmMRI+DLR
Depth of invasion (mm)	3.12 (2.44–3.81)	<.001	3.82 (3.10–4.55)	.004	4.07 (3.35–4.80)
Degree of contact with intracavernous ICA					
Total encasement	9 (13.4%)	<.001	13 (19.4%)	.02	25 (37.3%)
>270°	11 (16.4%)	<.001	15 (22.4%)	.04	26 (38.8%)
>180°	17 (25.4%)	.001	21 (31.3%)	.11	30 (44.8%)

<sup>a</sup> P value was calculated by using paired *t* test for depth of invasion and McNemar test for degree of contact with the intracavernous ICA. Data are mean or number of patients, and data in parentheses are 95% confidence intervals unless otherwise specified.



**FIG 3.** A 60-year-old woman who underwent a combined MR imaging protocol for preoperative evaluation of pituitary adenoma. On a 3-mmMRI, coronal, contrast-enhanced T1-weighted image (A), the tumor is present beyond the medial intercrotid line but not beyond the median intercrotid line (modified Knosp classification 1) and is <180° in contact with the intracavernous ICA. One-mmMRI, coronal, contrast-enhanced T1-weighted image (B) was reconstructed with DLR (C), and the tumor is shown to extend beyond the median intercrotid line (modified Knosp classification 2) and is <270° in contact with the intracavernous ICA (arrows).

mmMRI+DLR (30/67, 44.8%) than on 3-mmMRI (17/67, 25.4%; *P* = .001). Figure 3 demonstrates greater depth of invasion and degree of contact in relation to the ICA on 1 mm-MRI+DLR compared with 3-mmMRI and 1-mmMRI.

## DISCUSSION

In this prospective study, 1-mmMRI+DLR showed higher diagnostic performance in preoperatively predicting cavernous sinus

invasion by pituitary adenomas than 3-mmMRI. In addition, pituitary adenomas showed greater depth of invasion and a higher degree of contact in relation to the carotid artery on 1-mmMRI+DLR than on 3-mmMRI. This finding illustrates that thin-slice pituitary MR imaging with DLR allows better delineation of the morphologic relationship in the sellar fossa and achieves high spatial resolution with the relatively high signal-to-noise ratio that is required to accurately diagnose cavernous sinus invasion preoperatively.

Attempts to improve the radiologic accuracy of diagnosing cavernous sinus invasion by pituitary adenoma included the use of proton density-weighted imaging for identifying defects in the medial wall of the cavernous sinus<sup>14</sup> as well as a 3D spin-echo sequence,<sup>15</sup> volumetric interpolated brain examination,<sup>16</sup> and contrast-enhanced sampling perfection with application-optimized contrasts by using different flip angle evolutions.<sup>17</sup> Moreover, a radiomics approach using contrast-enhanced T1- and T2-weighted imaging showed better diagnostic performance than the clinico-radiologic models, and the diagnostic performance with an AUC of up to 0.83 on the test set was reported.<sup>13</sup> However, these approaches require additional image sequences with no established protocols and parameters or heavy post-imaging processing and analysis. On the other hand, DLR can be easily applied to the commonly used 2D spin-echo sequence, with rapid processing time enabling high spatial resolution without compromising image quality by image denoising with sharp edges and reduced artifacts. Our study showed that 43% of patients had pituitary adenomas with cavernous sinus invasion by the reference standard, which was higher than that previously reported of up to 21%,<sup>8,18,19</sup> and this result may be due to

the tertiary nature of the study center with a high prevalence of large, invasive pituitary adenomas. This was detected with 69% sensitivity using 1-mmMRI+DLR, and the diagnostic performance of 1-mmMRI+DLR was higher than that of 3-mmMRI in preoperatively predicting cavernous sinus invasion. While patients in this study underwent a combined imaging protocol of 1-mmMRI+DLR and 3-mmMRI, 1-mmMRI+DLR offers a better diagnostic value than 3-mmMRI without compromising image quality and may be considered to potentially replace 3-mmMRI.

The most widely used grading system for evaluating the parasellar extension of pituitary adenomas proposed by Knosp et al<sup>8</sup> and later modified by Micko et al<sup>9</sup> relies on the circular cuts of ICAs on the coronal section and uses the medial, median, and lateral lines drawn between the intracavernous and supracavernous ICAs. By increasing the number of slices that allows simultaneous visualization of the intracavernous and supracavernous ICAs, 1-mmMRI+DLR might allow more detailed evaluation of parasellar extension of the tumor in relation to the intercarotid lines and intracavernous ICA. In addition, 1-mmMRI+DLR may enable delineation of the presence of tumor at the lateral aspect of the intracavernous ICA. This accounted for the greater depth of invasion and higher proportion of pituitary adenomas with a greater degree of contact with the intracavernous ICA and grade IV tumors using 1-mmMRI+DLR, though it also resulted in false-positive cases. In addition, there was 1 case of pituitary adenoma with the tumor present lateral to the lateral intercarotid line at the superior cavernous compartment, which was made less conspicuous on 1-mmMRI+DLR by negating the partial volume average effect. In our study, 1-mmMRI+DLR showed higher diagnostic performance than 3-mmMRI in grade 3B and 4 pituitary adenomas according to the modified Knosp classification, whereas no significant difference was seen between 1-mmMRI+DLR and 3-mmMRI in pituitary adenomas with grades 3A, 3B, and 4. This finding supports 1-mmMRI+DLR as possibly being useful in using the modified Knosp classification with differentiation of involvement into the superior and inferior compartments of the cavernous sinus.

There are several limitations in this study. First, this was a single-center study with a relatively small sample size, so a multicenter validation with a larger cohort is required. Second, image analysis was performed by a single reader, which was practically inevitable in this prospective study design. We ensured that the blinded image analysis was performed before surgical resection and the image analysis was in accordance with the previous study that demonstrated good interobserver agreement in diagnosing cavernous sinus invasion.<sup>11</sup> Third, there is no established reference standard for determining cavernous sinus invasion by pituitary adenoma, so the reference standard was established by incorporating radiologic, intraoperative, pathologic, and laboratory findings.

## CONCLUSIONS

For preoperative prediction of cavernous sinus invasion by pituitary adenoma, 1-mmMRI+DLR showed higher diagnostic performance and demonstrated greater depth of invasion and degree of contact in relation to the carotid artery compared with 3-mmRI. This finding supports the diagnostic value of thin-slice pituitary imaging with DLR, though further validation in a multicenter study with a larger cohort is required.

Disclosures: Joonsung Lee—UNRELATED: Employment: employee of GE Healthcare; Marc R. Lebel—UNRELATED: Employment: employee of GE Healthcare; Stock/Stock Options: GE Healthcare.

## REFERENCES

1. Chuang CC, Lin SY, Pai PC, et al. **Different volumetric measurement methods for pituitary adenomas and their crucial clinical significance.** *Sci Rep* 2017;7:40792 [CrossRef Medline](#)
2. Roelfsema F, Biermasz NR, Pereira AM. **Clinical factors involved in the recurrence of pituitary adenomas after surgical remission: a structured review and meta-analysis.** *Pituitary* 2012;15:71–83 [CrossRef Medline](#)
3. Nishioka H, Fukuhara N, Horiguchi K, et al. **Aggressive transsphenoidal resection of tumors invading the cavernous sinus in patients with acromegaly: predictive factors, strategies, and outcomes.** *J Neurosurg* 2014;121:505–10 [CrossRef Medline](#)
4. Vieira JO Jr, Cukiert A, Liberman B. **Evaluation of magnetic resonance imaging criteria for cavernous sinus invasion in patients with pituitary adenomas: logistic regression analysis and correlation with surgical findings.** *Surg Neurol* 2006;65:130–35; discussion 135 [CrossRef Medline](#)
5. Kitano M, Taneda M, Shimono T, et al. **Extended transsphenoidal approach for surgical management of pituitary adenomas invading the cavernous sinus.** *J Neurosurg* 2008;108:26–36 [CrossRef Medline](#)
6. Chang EF, Zada G, Kim S, et al. **Long-term recurrence and mortality after surgery and adjuvant radiotherapy for nonfunctional pituitary adenomas.** *J Neurosurg* 2008;108:736–45 [CrossRef Medline](#)
7. Greenman Y, Ouaknine G, Veshchev I, et al. **Postoperative surveillance of clinically nonfunctioning pituitary macroadenomas: markers of tumour quiescence and regrowth.** *Clin Endocrinol (Oxf)* 2003;58:763–69 [CrossRef Medline](#)
8. Knosp E, Steiner E, Kitz K, et al. **Pituitary adenomas with invasion of the cavernous sinus space: a magnetic resonance imaging classification compared with surgical findings.** *Neurosurgery* 1993;33:610–17; discussion 617–18 [CrossRef](#)
9. Micko AS, Wöhrer A, Wolfsberger S, et al. **Invasion of the cavernous sinus space in pituitary adenomas: endoscopic verification and its correlation with an MRI-based classification.** *J Neurosurg* 2015;122:803–11 [CrossRef Medline](#)
10. Varrassi M, Cobiachi Bellisari F, Bruno F, et al. **High-resolution magnetic resonance imaging at 3T of pituitary gland: advantages and pitfalls.** *Gland Surg* 2019;8:S208–15 [CrossRef Medline](#)
11. Kim M, Kim HS, Kim HJ, et al. **Thin-slice pituitary MRI with deep learning-based reconstruction: diagnostic performance in a post-operative setting.** *Radiology* 2021;298:114–22 [CrossRef Medline](#)
12. Lebel RM. **Performance characterization of a novel deep learning-based MR image reconstruction pipeline.** *arXiv.org* 2020 <https://arxiv.org/abs/2008.06559>. Accessed March 18, 2021
13. Niu J, Zhang S, Ma S, et al. **Preoperative prediction of cavernous sinus invasion by pituitary adenomas using a radiomics method based on magnetic resonance images.** *Eur Radiol* 2019;29:1625–34 [CrossRef Medline](#)
14. Cao L, Chen H, Hong J, et al. **Magnetic resonance imaging appearance of the medial wall of the cavernous sinus for the assessment of cavernous sinus invasion by pituitary adenomas.** *J Neuroradiol* 2013;40:245–51 [CrossRef Medline](#)
15. Lien RJ, Corcuera-Solano I, Pawha PS, et al. **Three-Tesla imaging of the pituitary and parasellar region: T1-weighted 3-dimensional fast spin echo Cube outperforms conventional 2-dimensional magnetic resonance imaging.** *J Comput Assist Tomogr* 2015;39:329–33 [CrossRef Medline](#)
16. Davis MA, Castillo M. **Evaluation of the pituitary gland using magnetic resonance imaging: T1-weighted vs. VIBE imaging.** *Neuroradiol J* 2013;26:297–300 [CrossRef Medline](#)
17. Wu Y, Wang J, Yao Z, et al. **Effective performance of contrast enhanced SPACE imaging in clearly depicting the margin of pituitary adenoma.** *Pituitary* 2015;18:480–86 [CrossRef Medline](#)
18. Hofstetter CP, Nanaszko MJ, Mubita LL, et al. **Volumetric classification of pituitary macroadenomas predicts outcome and morbidity following endoscopic endonasal transsphenoidal surgery.** *Pituitary* 2012;15:450–63 [CrossRef Medline](#)
19. Cottier JP, Destrieux C, Brunereau L, et al. **Cavernous sinus invasion by pituitary adenoma: MR imaging.** *Radiology* 2000;215:463–69 [CrossRef Medline](#)